Project Title: Influence of Wetting and Mass Transfer Properties of Organic Chemical Mixtures in Vadose Zone Materials on Groundwater Contamination by Nonaqueous Phase Liquids.

Project PI: Charles Werth
Department of Civil and Environmental Engineering
University of Illinois at Urbana-Champagin
205 North Mathews Ave., MC-250
Urbana, IL 61801

Project co-PIs: Albert Valocchi, Hongkyu Yoon, Univ. of Illinois
Mart Oostrom, PNNL

Objectives:
Previous studies have found that organic acids, organic bases, and detergent-like chemicals change surface wettability. The wastewater and NAPL mixtures discharged at the Hanford site contain such chemicals, and their proportions likely change over time due to reaction-facilitated aging. The specific objectives of this work were to 1) determine the effect of organic chemical mixtures on surface wettability, 2) determine the effect of organic chemical mixtures on CCl_4 volatilization rates from NAPL, and 3) accurately determine the migration, entrapment, and volatilization of organic chemical mixtures.

Tasks:
Five tasks were proposed to achieve the project objectives. These are to 1) prepare representative batches of fresh and aged NAPL-wastewater mixtures, 2) to measure interfacial tension, contact angle, and capillary pressure-saturation profiles for the same mixtures, 3) to measure interphase mass transfer rates for the same mixtures using micromodels, 4) to measure multiphase flow and interphase mass transfer in large flow cell experiments, all using the same mixtures, and 5) to modify the multiphase flow simulator STOMP in order to account for updated P-S and interphase mass transfer relationships, and to simulate the impact of $CCl4$ in the vadoze zone on groundwater contamination.

Highlights:
Major results identified in this work are discussed in the Project Activities, Results and Findings section below. All publications from this work are listed at the end of the report.

Personnel:
Project funding began in March of 2006. All personnel appointed to the project, appointment dates, and tasks that they focused on are in Table 1 below. One graduate student (Scott Nellis) performed the work in Tasks 1 and 2, with help from a part-time post doc (Changyong Zhang) and co-PI Hongkyu Yoon. Scott's work resulted in two publications, one in Vadose Zone Journal (VZJ) and one in Environmental Science and Technology (ES&T). Two graduate students (Garvin Prescod and Karl DeHoff) performed most of the work in Task 3, with some assistance from Changyong Zhang, an undergraduate researcher (Paul Biretta), and a graduate student (Mike Fanizza). Garvin focused on measuring DNAPL mass transfer under various conditions,

while Karl focused on measuring mineral precipitation reactions relevant to DNAPL remediation. This work resulted in a publication in ES&T that received a best paper award in 2010. Garvin Prescod and Hongkyu Yoon performed most of the large-scale flow cell experiments in Task 4, and Hongkyu Yoon with assistance from a part-time graduate student (Luke Fitzgerald) performed the work in Task 5. This work resulted in 2 publications in Journal of Contaminant Hydrology (JCH), one publication in Water Resources Research, and another manuscript that will soon be submitted to JCH.

Table 1. Personnel appointed to project, time of appointment, and task(s) assigned.

Position	Personnel	Dates on Project	Tasks
PIs:	Charles Werth	Not Applicable	1-5
	Albert Valocchi	Not Applicable	1-5
	Hongkyu Yoon	12/06-5/10	4-5
Post-Doc:	Changyong Zhang	3/07-10/09 (half time)	2 and 3
Grad. Students:	Scott Nellis	7/06-5/08	1 and 2
	Garvin Prescod	8/06-5/08	3 and 4
	Karl DeHoff	8/08-5/10	3
	Luke Fitzgerald	8/09-5/11 (half time)	5
	Mike Fanizza	1/11-3/11	3
Undergrad. Student:	Paul Biretta	1/09-5/10 (hourly)	Task 3

Project Activities, Results, and Findings:
Task 1: Our first task was preparing representative batches of fresh and aged NAPL/wastewater mixtures for use in the remaining tasks. Aging refers to mixtures that have been allowed to incubate at room temperature for weeks to months in the absence and presence of microorganisms from the Hanford site. Four different unique batches were prepared: MIX1, MIX2, MIX3, and MIX4. MIX1 contains the major organic and wastewater components reported to be disposed of at the Hanford site. MIX2 contains these same components plus tributyl phosphoric acid (TBP) and bis (2-ethyl-hexyl) phosphate (D2EHP). MIX3 contains MIX2 components plus the organic base dodecylamine (DDA) in the wastewater. Finally, MIX4 contains the MIX1 components with dibutyl phosphoric acid (DBP) substituted for TBP because it is reasoned that DBP is a degradation product of TBP. We also created two binary mixtures (MIX5 and MIX6) to investigate the effects of lard oil (LO) and dibutyl-butyl phosphonate (DBBP) on carbon tetrachloride (CT) separately. The compounds used to create MIX1-4 are based on reports that list major NAPL (Rohay et al., 1994) and wastewater (Last and Rohay, 1993) components at the Hanford site. The major NAPL components of all mixtures (including two binary mixtures) are listed in Table 2; the major wastewater components are listed in Table 3.

After preparing the six mixtures, we aged MIX1 for weeks to months in the absence of biological activity. We also evaluated biological aging by preparing an enrichment culture from sediments obtained from the Hanford site, by acclimating this culture to grow on MIX1, and by allowing biodegradation of MIX1 to occur for different time periods and under different conditions. When biological growth on MIX1 in the presence of Hanford sediments was apparent from increases in turbidity, supernatant in the sediment/water/MIX1 systems was transferred to

sediment free bottles with only MIX1 and additional time was allowed for biological reaction/aging. Interfacial properties of chemically and biologically aged MIX1 were measured on chemically and biologically aged samples as part of Task 2. Additional mixtures were not chemically or biologically aged because chemical and interfacial properties of MIX1 were found to be similar to those of the other mixtures.

Table 2. Summary of mixture compositions (% by volume).

Mixture	CT	DBBP	TBP	DBP	LO	D2EHP	Density (kg/m^3)
MIX1	73.6	14.7	8.8	-	2.9	-	1.424
MIX2	72.9	14.5	8.7	-	2.9	1.0	1.445
MIX3†	72.9	14.5	8.7	-	2.9	1.0	1.443
MIX4	73.6	14.7	1.5	7.3	2.9	-	1.457
MIX5	97.1	-	-		2.9	-	1.586
MIX6	85.0	13.5	1.5		-	-	1.509

† The wastewater phase of MIX3 contains 10^{-3} M dodecylamine (DDA).
CT, DBBP, TBP, LO, D2EHP represent carbon tetrachloride, dibutyl butyl phosphonate, tributyl phosphate, machining lard oil, and bis (2-ethyl-hexyl) phosphate, respectively.

Table 3. Major wastewater components of mixtures.

Wastewater phase pH = 2.5	M nitrate
Compound	[mol/L]
65-70% HNO_3	2.5
Aluminum Nitrate Nonahydrate	0.625
Magnesium Nitrate Hexahydrate	0.625
Calcium Nitrate Tetrahydrate	0.625
Sodium Nitrate	0.625
Total Waste Water Phase	5

Task 2: Our second task was measuring interfacial tension, contact angle, and capillary-pressure saturation profiles for all NAPL/wastewater mixtures. Experiments initially focused on measuring surface and interfacial tensions and contact angles for the non-biologically aged mixtures, surface and interfacial tensions for chemically aged MIX1, and surface and interfacial tensions for the biologically aged MIX1. Interfacial tension was measured for air-water, air-organic, and water-organic systems using the pendant drop method with a goniometer. In this method, a drop is suspended from the edge of a flat needle and images are collected over time. Experimental procedures and results were reported in a master student's thesis (Nellis, 2008). The results and interpretation of surface and interfacial tension measurements of the non-biologically aged mixtures (MIX1-MIX6) were published in Vadose Zone Journal (Nellis et al., 2009). These results were used to evaluate alternative models for predicting surface and interfacial tensions of complex mixtures. Modeling results were published in Environmental Science and Technology (Yoon et al., 2009). Below, we briefly report these findings, as well as those for biologically aged mixtures and contact angles. Surface and interfacial tension results

for chemically aged MIX1 are not reported because we found that this aging had no significant effect on interfacial properties.

Surface and interfacial tension results for the different mixtures and wastewater are shown in Figure 1. They show that the addition of the surface active components to CT caused a significant lowering of the interfacial tension with water or wastewater and the surface tension of the wastewater phase in equilibrium with the organic mixtures, compared to pure CT, but had minimal effect on the surface tension of the NAPL itself. As shown in Figure 2, these results lead to large differences in spreading coefficients for several mixtures, where the additives caused both a higher (more spreading) initial spreading coefficient and a lower (less spreading) equilibrium spreading coefficient. This indicates that if these mixtures migrate into uncontaminated areas, they will tend to spread quickly, but form a higher residual NAPL saturation after equilibrium, as compared to pure CT. Over time, CT likely volatilizes more rapidly than other components in the originally disposed mixtures and the lard oil and phosphates would become more concentrated in the remaining NAPL, resulting in a lower interfacial tension for the mixture. Spreading coefficients are expected to increase and perhaps change the equilibrated organic mixtures from nonspreading to spreading in water-wetting porous media. These results show that the behavior of organic chemical mixtures should be accounted for in numerical flow and transport models.

A comprehensive comparison of thermodynamic and empirical models for estimating interfacial tension of organic mixtures with water was conducted, mainly focusing on chlorinated organic compounds for 14 ternary systems, three quaternary systems, and one quinary system. Emphasis was placed on novel results for systems with three and four organic chemical compounds, and for systems with composite organic compounds like lard oil and mineral oil (e.g., like the mixtures disposed of at the Hanford site). Seven models were evaluated: the ideal and nonideal monolayer models (MLID and MLNID), the ideal and nonideal mutual solubility models (MSID and MSNID), an empirical model for ternary systems (EM), a linear mixing model based on mole fractions (LMMM), and a newly developed linear mixing model based on volume fractions of organic mixtures (LMMV) for higher order systems. As shown in Figure 3, the two ideal models (MLID and MSID) fit ternary systems of chlorinated organic compounds without surface-active compounds relatively well. However, both ideal models did not perform well for the mixtures containing a surface-active compound. However, for these systems, both the MLNID and MSNID models matched the interfacial tension data well. It is shown that the MLNID model with surface coverage value (0.00341 mmol/m^2) obtained in this study can practically be used for chlorinated organic compounds. The LMMM poorly estimated the interfacial tension as the difference in interfacial tension values of individual organic compounds in a mixture increases. The EM with two fitting parameters provided accurate results for all 14 ternary systems including composite organic compounds. The new LMMV method for quaternary and higher component systems was successfully tested. This study shows that the LMMV may be able to be used for higher component systems where molar volume changes due to mixing are relatively small. The LMMV was incorporated into a multiphase flow and transport model, STOMP (Subsurface Transport Over Multiple Phases), which was used in Task 5.
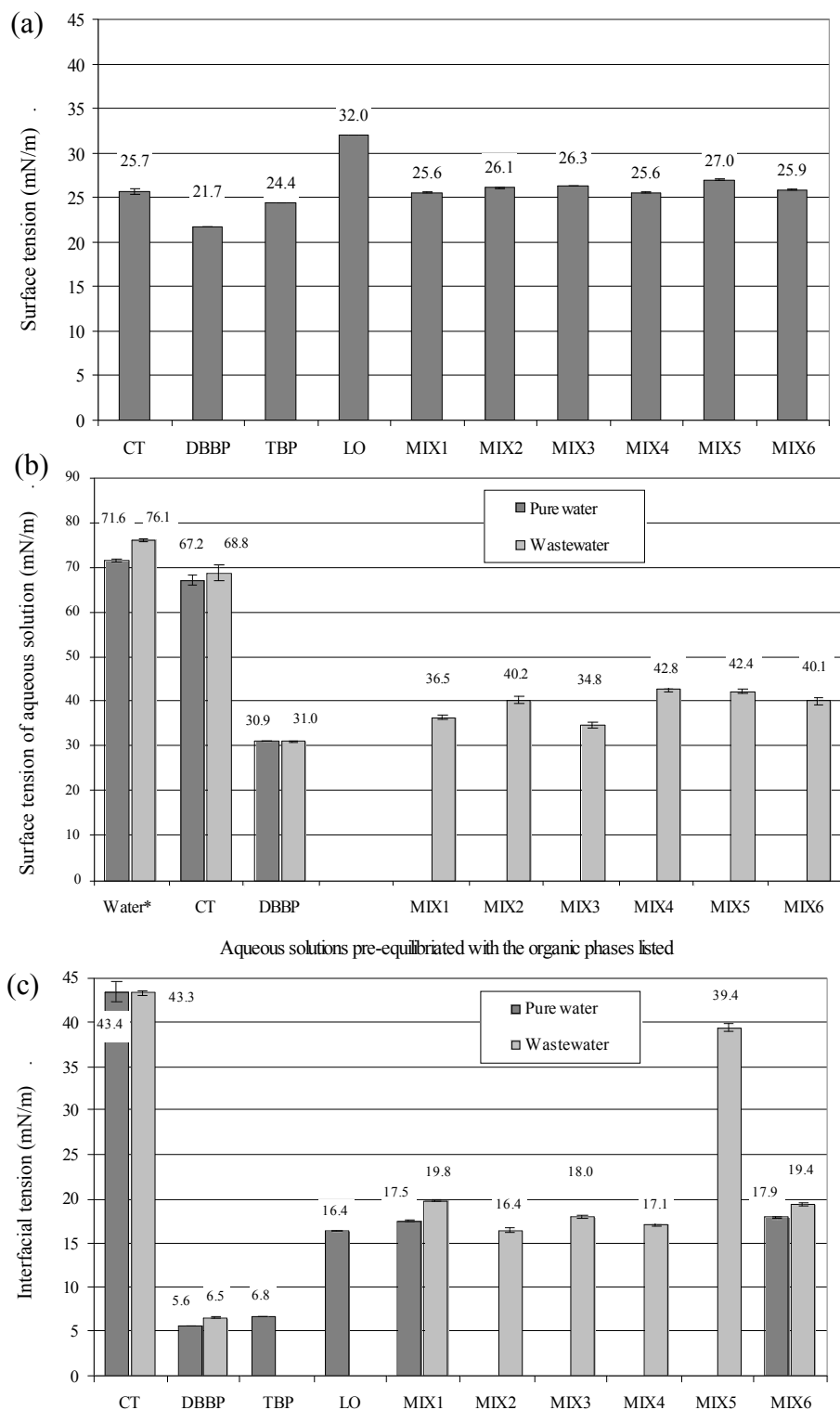
Figure 1. (a) Surface tension of organic phase, (b) surface tension of aqueous phase, and (c) organic-aqueous interfacial tension. All aqueous and organic phases were pre-equilibrated, except Water* (pure water and wastewater). Bars on the chart represent 95 % confidential intervals.
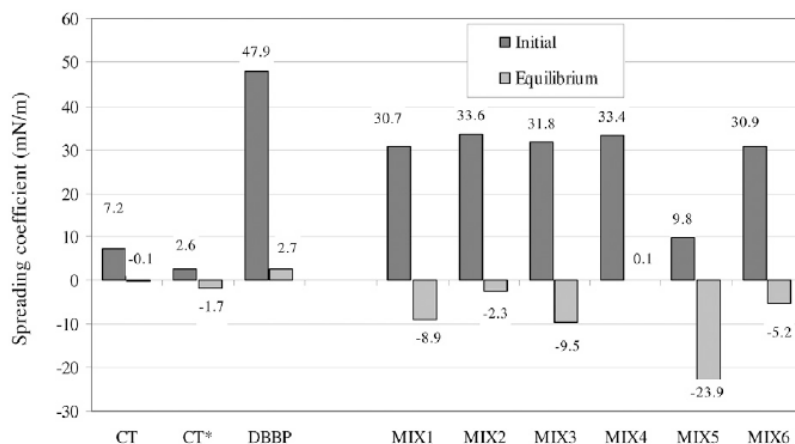
Figure 2. Initial and equilibrium spreading coefficients for the organic compounds CT, DBBP, and six organic mixtures (MIX1-MIX6) and wastewater, and the spreading coefficient for CT and pure water (CT*).
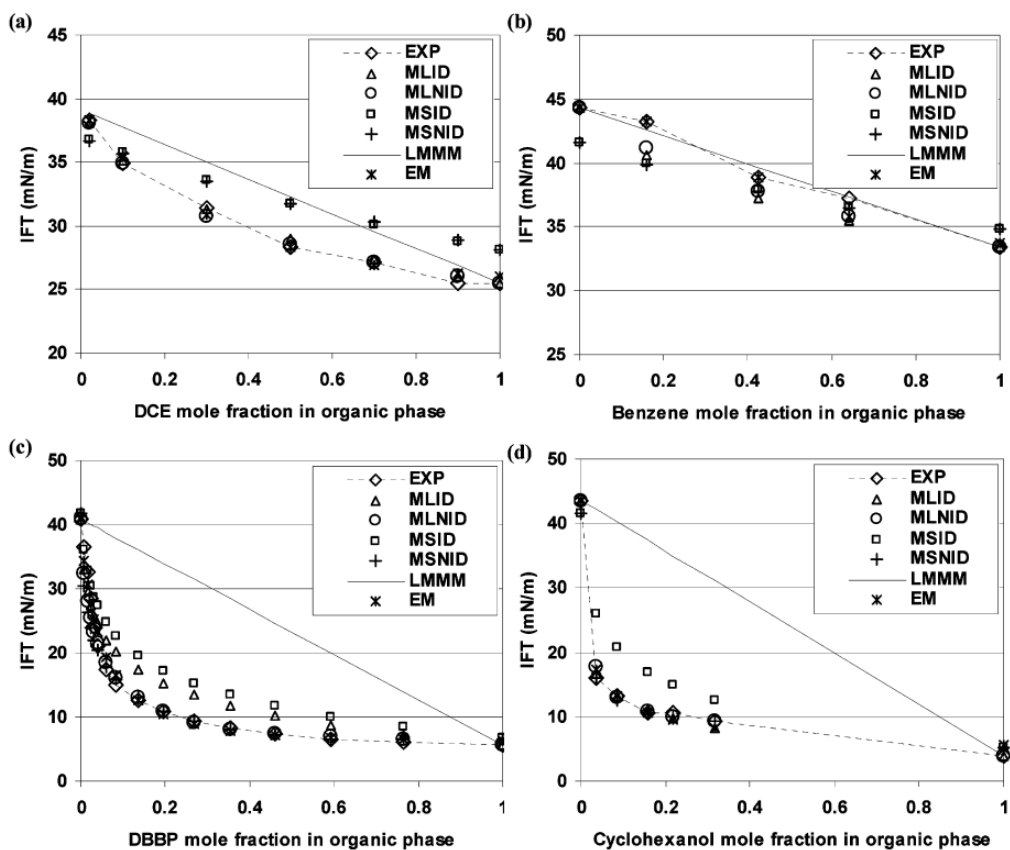

Figure 3. Measured and estimated interfacial tension values for ternary systems of (a) DCE-TCE-water, (b) Benzene-CT-water, (c) DBBP-CT-water, and (d) cyclohexanol-CT-water (DCE=dichloroethene, TCE=trichloroethene, EXP: experimental, MLID: ideal monolayer model, MLNID: nonideal monolayer model, MSID: ideal mutual solubility model, MSNID: nonideal mutual solubility model, LMMM: linear mixing model based on mole fraction, EM: empirical model).

The biological activity for the aged MIX1 was measured by UV absorbance. Three rounds of biological aging experiments were conducted where adjustments were made in an effort to increase reproducibility and increase levels of biological growth. The UV absorbance showed biological growth in all MIX1 samples with several different conditions (results not shown). A brief description of each round is presented in the caption of Figure 4. The surface and interfacial tension values are shown for all 3 rounds in Figure 4. The resulting tension values from all three rounds are comparable. The highest growing experiments in round 3, where the sediment bottles were aerated for 4 days prior to transfer to UV bottles, showed the lowest interfacial tension value, but did not differ by very much compared to the round 2 value where there was significantly less growth captured by UV spectrometry. The interfacial tension decreased from the measured value of un-aged MIX1 and pure water (17.5 mN/m) to the range of 10.7-15.4 mN/m. In a similar set of experiments by Powers et al. (2003), they found that the interfacial tension did not decrease below 10 mN/m. They observed a more significant drop of interfacial tension (i.e., 2-3 mN/m) in a PCE-TCE mixture obtained from the subsurface at the U.S. DOE Savannah River Site, due to precipitation of metal species at the interface between DNAPL and water forming a semi-rigid film at high DNAPL to water volume ratios. Clifford et al. (2007) also showed that anionic biosurfactants (i.e., Rhamnolipids) can lower the interfacial tension of PCE from 45 to 10 mN/m, resulting in the increase in the solubility of PCE from 250 mg/L to 365 mg/L. Hence, results in this study show that the biological activity may not significantly affect the interfacial tension of CT mixtures due to the presence of surface active compounds in the mixtures. However, the decrease of interfacial tension due to both the presence of surface active compounds and biological activities may increase the solubility of CT compared to the solubility of CT estimated from Roults' law.
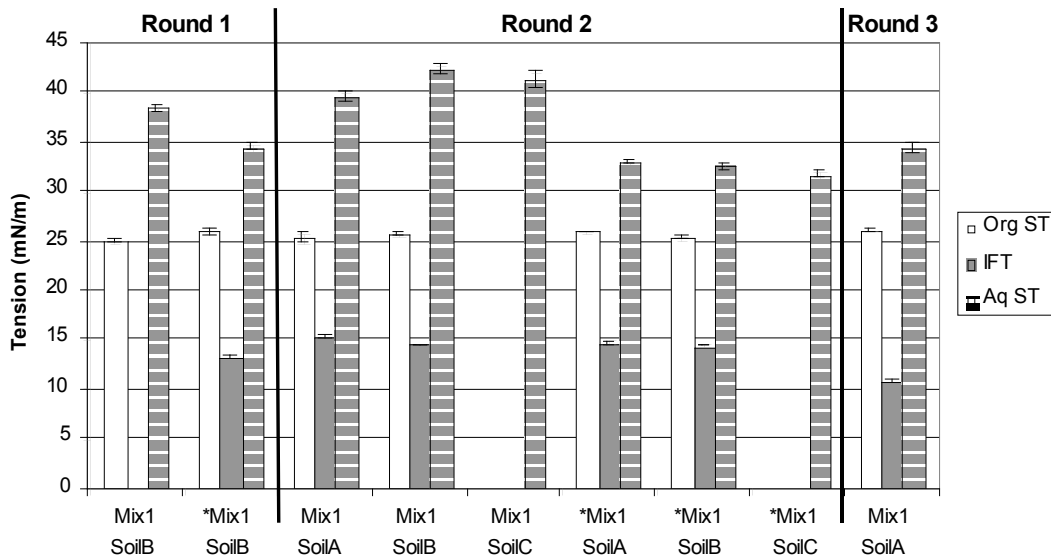

Figure 4. Surface and interfacial tensions for bio-aging experiments. *Mix1 was prepared from mineral media aged in the saturated Mix1 bottle for 140 hours. For round 1, mineral media was first aerated, equilibrated with MIX1, and then added to soil B. For round 2, mineral media was first equilibrated with MIX1, added to three different soils (A,B, and C), and then aerated. For round 3, the mineral media of Mix1 SoilA at 961 hours from round 2 was replaced and the

replaced media was aerated for 4 days. For rounds 1, 2, and 3, the tension measurements were conducted after 355 hours, 135 hours, and 240 hours aging, respectively.

Contact angles were also measured with the goniometer. Briefly, polished and thoroughly cleaned quartz and calcite surfaces were pre-equilibrated with either the (waste)water or the NAPL mixture for 72 hours. Next, the slides were removed from the pre-equilibration fluid, immersed in a new (waste)water mixture, and then a small drop of NAPL mixture was placed on the slide and the contact angle was measured from a photograph of the drop. Results for pure CT and MIX1 are shown in Figure 5. For pure CT, results from replicates and different pre-equilibration fluids show good agreement for both quartz and calcite slides. For MIX1, results from replicates and different pre-equilibration fluids show higher confidential intervals, indicating more heterogeneous interactions between MIX1 and surfaces. Unlike the case of pure CT, MIX1 does change the wettability of the quartz surface from water wetting to neutral wetting and the wettability of the calcite surface from water wetting to oil wetting. Since capillary pressure is directly related to the contact angle, this finding could have a significant impact on the fate of the Hanford mixture that would be otherwise not present in the case of a pure phase CT spill.
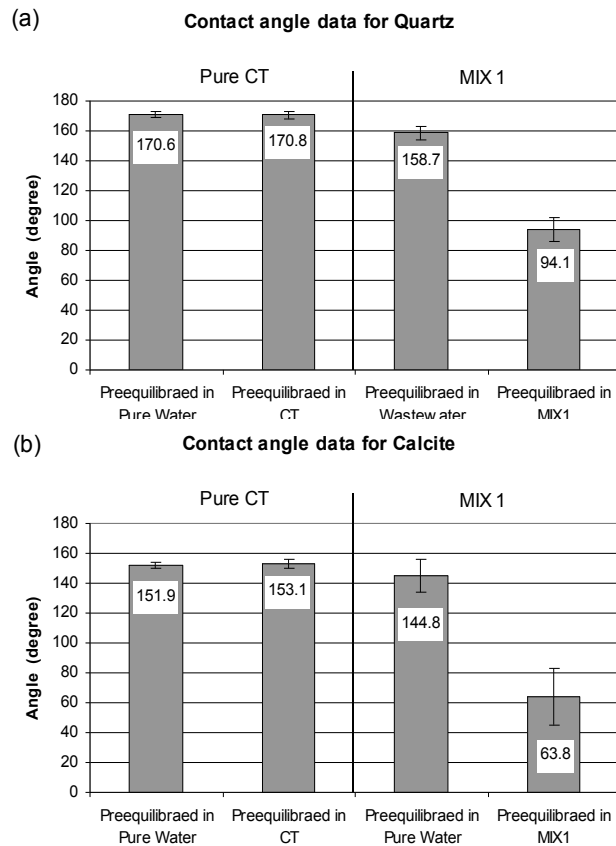

Figure 5. Contact angle measurements for (a) quartz slides and (b) calcite slides pre-equilibrated with water or MIX1. Bars on the chart represent 95 % confidential intervals.

Task 3: Our third task was fabricating micromodels and using them to measure entrapment, NAPL-air / NAPL-water interfacial areas, flow dynamics in the presence of blocked pores, and mass transfer rates of volatilization and dissolution. We used homogeneous micromodels to perform NAPL entrapment and dissolution experiments for pure CT and the MIX1 NAPL, and to perform dynamic flow experiments where pores were blocked with mineral precipitates of relevance to NAPL remediation efforts. Homogeneous micromodels contain a pore network approximately 2 cm long by 1 cm wide, and have a staggered array of homogeneous circular silicon posts (300 μm in diameter) spaced 40 μm apart at the closest points. For NAPL mass transfer experiments, we performed thresholding and image analysis to quantify differences in blob size with entrapment and dissolution. For the dynamic flow experiments, we used laser confocal microscopy to evaluate pore blocking my minerals, and we used Raman spectroscopy to evaluate mineral phases. Results from these experiments are summarized below.

Snapshots of entrapped NAPL for pure CT and MIX1 during NAPL dissolution are shown in Figure 6. NAPL was introduced from the left hand side of the micromodel and water was introduced at a flow rate of 40 ml/hr from the right hand side. As shown in 6(a) and 6(c), CT has more connected patterns than MIX1, and this is attributed to different viscosity and interfacial tension values. MIX1 has a higher viscosity (1.5 cp) than pure CT (0.97 cp), and the initial interfacial tension of MIX1 (17.5 mN/m) is lower than pure CT (43.4 mN/m). The effect of

(a) CT 6 hrs

(c) MIX1 1 hr

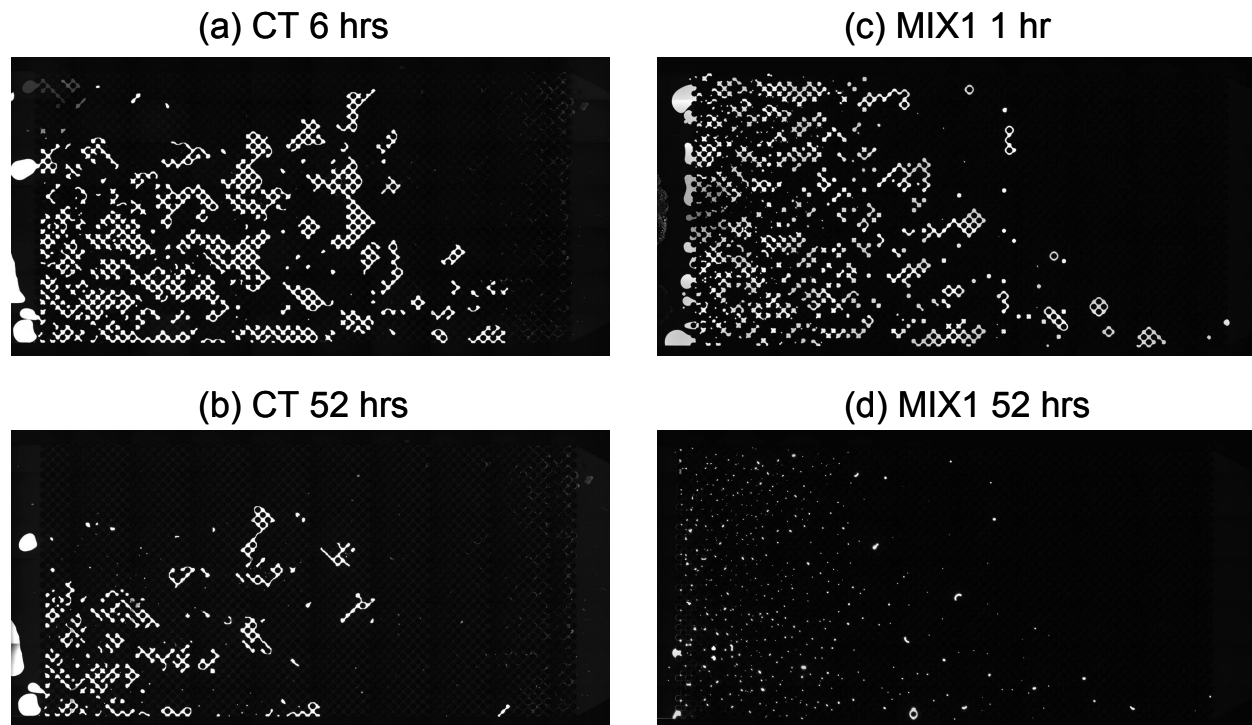### (b) CT 52 hrs

(d) MIX1 52 hrs

Figure 6. Snapshots of NAPL profiles in micromodel experiments at different times for pure CT and MIX1.

these parameters can be characterized by the capillary number (the ratio of viscous forces (velocity x viscosity of aqueous phase) to capillary forces (interfacial tension)). The capillary number for MIX 1 is larger than that for pure CT, and larger capillary numbers have been

correlated to smaller NAPL blob sizes (Ng and Payatakes, 1980). After 52 hrs, pure CT dissolved from most upstream regions with highly connected CT blobs, while MIX1 has much smaller size blobs left. This is also attributed to the larger capillary number, or lower interfacial tension, of MIX1 compared to pure CT. A lower interfacial tension favors the breakup of blobs during dissolution.

Total NAPL area and perimeter length for the dissolution experiments presented in Figure 6 are shown in Figure 7. The total NAPL volume is equal to the total NAPL area multiplied by the micromodel depth, and the total NAPL interfacial area is equal to the total NAPL perimeter length multiplied by the micromodel depth. The initial total NAPL area of MIX1 was slightly lower than that of pure CT, while initial perimeter length of MIX1 was higher than that of pure CT. As a result, initial NAPL dissolution was higher for MIX1 than for pure CT. The presence of high solubility DBBP (~1200 mg/L) in MIX1 may result in fast NAPL dissolution at the beginning. Since MIX1 has more small NAPL blobs than CT, the overall NAPL dissolution rate was faster in MIX1 until a large fraction of high solubility components (DBBP and CT) in MIX1 dissolved. Like the NAPL distribution after 52 hrs in Figure 6, the NAPL dissolution rate in MIX1 decreased dramatically, probably due to a high fraction of TBP and LO remaining at late time due to their lower solubility relative to DBBP and CT. After approximately 60 hrs, MIX1 area and perimeter length decreased very slowly (Figure 7), while pure CT area and perimeter length decreased steadily.
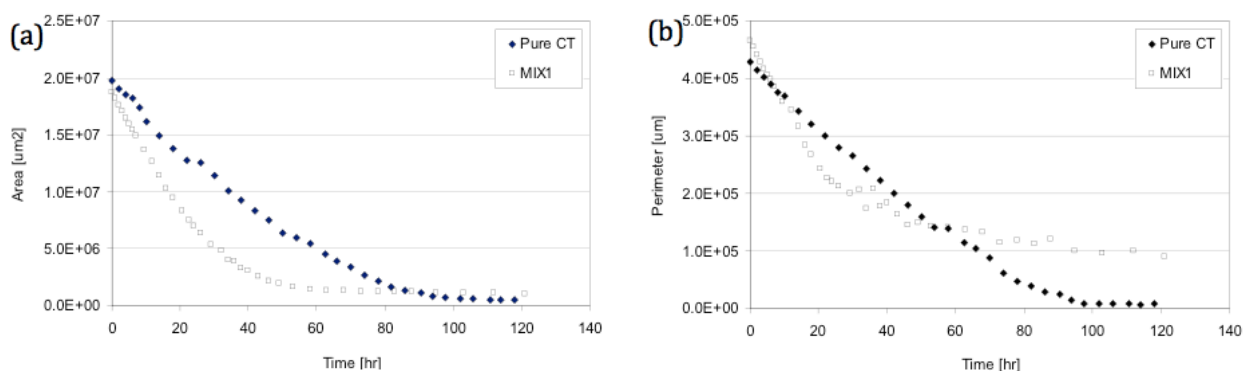

Figure 7. (a) Total surface area of NAPL profiles and (b) total perimeter of NAPL profiles over time. Total NAPL volume can be obtained as the product of total NAPL surface area and the depth of micromodel (38 μm) and total perimeter represents total interfacial area between NAPL and water.

Changes in flow dynamics and mass transfer that occur with blocked pores was investigated by introducing solutions of $CaCl_2$ and Na_2CO_3 through two separate inlets into a homogeneous pore network, and measuring $CaCO_3$ precipitation and flow dynamics in the precipitation zone. Four different saturation states ($\Omega = [Ca^{2+}] [CO_3^{2-}] / K_{spCaCO3}$) were evaluated, and mineral precipitates in the pore structures are shown in Figure 8a. Precipitation rates increased and the total amount of precipitates decreased with increasing saturation state. Raman spectra of precipitates in the pore structure were obtained (Figure 8b), and it was determined that only vaterite and calcite crystals were formed (no aragonite). The relative amount of vaterite increased from 80% at the lowest saturation ($\Omega_v = 2.8$ for vaterite) state to 95% at the highest saturation

state ($\Omega_v = 4.5$). Fluorescent tracer tests conducted before and after $CaCO_3$ precipitation indicate that pore spaces were occluded by $CaCO_3$ precipitates along the transverse mixing zone between $CaCl_2$ and Na_2CO_3, that precipitates significantly reduced porosity and permeability, and that transverse diffusion/mixing through the blocked pores was reduced compared to open pores. The results suggest that mineral precipitation along plume margins during in situ remediation of NAPL in groundwater can decrease reactant mixing and cleanup efficiency. These results were published in ES&T (Zhang et al., 2010), and received a best paper award (top ten of 1500 papers in ES&T in 2010). Another manuscript is in preparation and will soon be submitted that explores pore scale modeling of mineral precipitation and flow dynamics (Yoon et al., 2011).
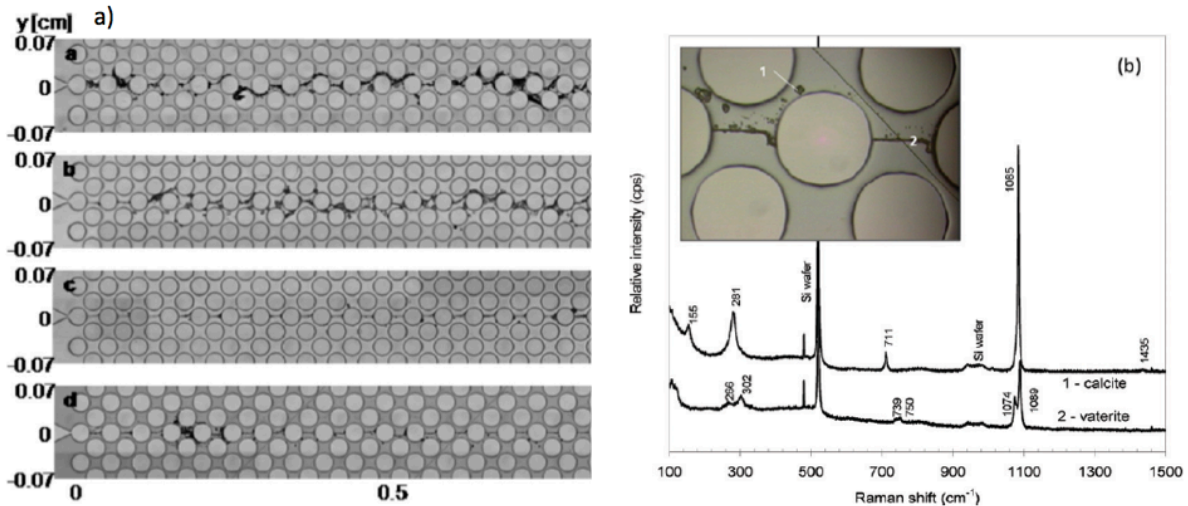

Figure 8. a) Images of center of micromodels with CaCO3 precipitates formed along the mixing zone at different saturation states (top) $\Omega c/\Omega v$) 3.4/2.8, (top center) $\Omega c/\Omega v$) 3.8/3.1, (bottom center) $\Omega c/\Omega v$) 4.6/3.9, and (bottom) $\Omega c/\Omega v$) 5.2/4.5. b) Laser confocal image of precipitate and Raman spectra of precipitate in pore structure.

Task 4: Our fourth task was analyzing multiphase flow during NAPL infiltration and interphase mass transfer during NAPL soil vapor extraction in 2D flow cell experiments. Experiments focused on conducting three different flow cell experiments in order to account for the impact of organic chemical mixtures and wastewater on DNAPL distribution and migration in a layered vadose zone, and to account for the difference of mass transfer processes between organic mixtures (MIX2) and pure CT. The 2D experiments were conducted in a 100-cm long, 80-cm high, and 5.5-cm wide glass walled flow cell, consisting of a stainless-steel frame, Teflon gaskets, and 0.375-cm thick glass walls. The flow cell contained a fine-grain sand layer (70 mesh), surrounded by medium-grain sand (20/30 mesh). The flow cell was packed under saturated conditions to a height of z = 40 cm. The water table was then lowered to z = 10 cm before remainder of the porous media were added to a height of z =75 cm. Both sands were premixed with water, approximately yielding irreducible water saturations. After the packing process was completed, a stainless-steel lid was placed on the flow cell to prevent the escape of water and NAPL vapors, and the water table was lowered to z = 2 cm. Either clean water or the aqueous phase wastewater in Task 1 was used. Either pure CT or Mix2 prepared in Task 1 was used; Mix 2 was used because it has a slightly lower DNAPL-water interfacial tension than the

other three mixtures (i.e., MIX1, MIX3, MIX4). Results from these experiments are presented with the numerical simulation results in Task 5.

Task 5: Our fifth task was to modify the multiphase flow simulator STOMP in order to account for the updated capillary pressure-saturation and interphase mass transfer relationships for multi-component NAPLs (i.e., mixture), and to simulate the impact of CT in the vadoze zone on groundwater contamination. STOMP was modified to account for the effect of chemical properties on capillary pressure-saturation using a scaling method implemented in STOMP (White et al., 2005). Capillary-pressure saturation profiles of air-water system for the Hanford soils in the literature were scaled based on measured surface and interfacial tensions and contact angles in Task 2. Modifications to incorporate kinetic mass transfer and multicomponent NAPL behavior into the STOMP simulator were completed by Pacific Northwest National Laboratory (Oostrom et al., 2008). In the paragraphs that follow, we present experiments flow cell results, corresponding STOMP results using the code that we modified, and STOMP results of field NAPL migration using calibration parameters obtained by fitting flow cell experiments.

The location and potential risk that NAPL mixture at the Hanford site pose to groundwater contamination remain unknown due to our poor understanding of surface-active chemical impacts on NAPL migration and entrapment. To address this, we monitored the migration and entrapment of pure CT and MIX2, respectively, in two separate flow-cell experiments. In both experiments, the flow cell was packed with a fine-grained sand lens surrounded by coarse-grained sand, all at residual water saturation. Pure water was used with pure CT, and wastewater characteristic of the Hanford site was used with the CT mixture. Equal volumes of either pure or mixture CT dyed red was released at the top of the flow cell, and NAPL migration was monitored using by taking photographs at selected time points during infiltration. The multiphase flow simulator STOMP was used to model the flow cell experiments using literature values of density, surface and interfacial tensions, and viscosity, and model calibration was performed by adjusting air entry pressure, pore size distribution, and residual NAPL saturation. Experimental and model results are shown in Figure 9. We observed that compared to pure CT, the CT mixture migrates downward more slowly, spreads more laterally during infiltration, and results in a higher residual NAPL saturation.   As a result, the CT mixture does not break through the fine sand barrier like the pure CT. For the CT mixture, downward migration is slower because the mixture has a lower density and higher viscosity than pure CT, spreading is greater because the mixture's initial spreading coefficient is larger than pure CT, and NAPL saturation is greater because the mixture's equilibrium spreading coefficient is more negative than pure CT. Model results adequately capture differences in pure and mixture CT migration, and the time evolution of the migrating NAPL fronts. These results are presented in a manuscript that will soon be submitted to Journal of Contaminant Hydrology (Fitzgerald et al., 2011).

Mechanisms that govern the removal of pure CT during soil vapor extraction (SVE) were evaluated by comparing results of a detailed data set from the aforementioned flow cell experiment (Task 4) with results from numerical and analytical model simulations. The pure CT (499 ml) was injected at the top of the flow cell and allowed to redistribute in the variably saturated system. A dual-energy gamma radiation system was used to determine the initial NAPL saturation profile in the fine-grained sand layer after NAPL migration ceased, and imaging results from this method are compared to a photograph of initial NAPL distribution in Figure 10.

Gas concentrations at the outlet of the flow cell and at 15 sampling ports inside the flow cell were measured during subsequent CT removal using SVE.
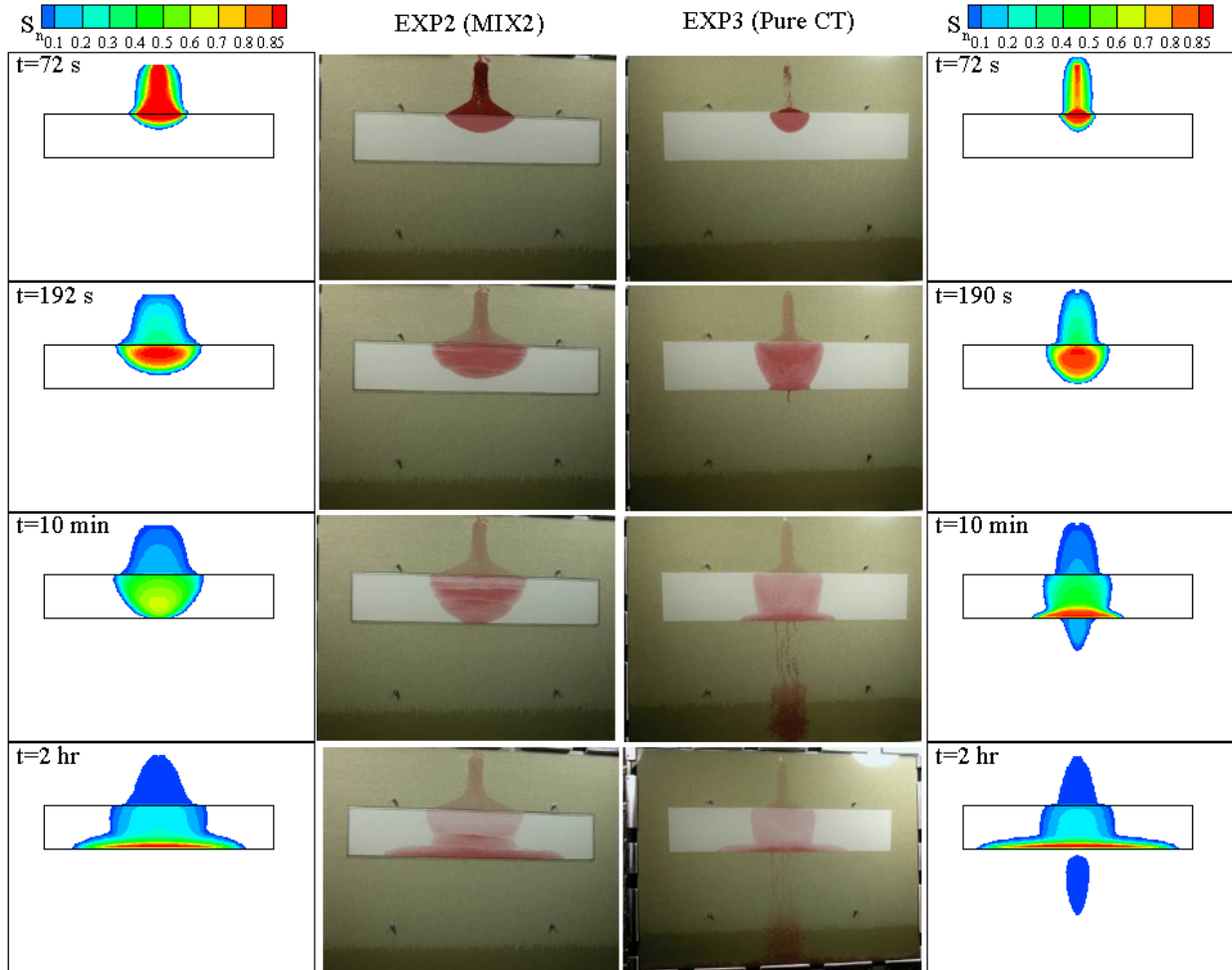

Figure 9. Photographic images and model simulations of pure NAPL migration into the flow cell.

Results show that CT mass was removed quickly in coarse-grained sand, followed by slow removal from the fine-grained sand layer. Photographs of dyed CT in the fine-grained sand layer at different times are shown Figure 11a. As shown in Figure 11b, fast removal of CT from the coarse-grained sand resulted in effluent gas concentrations that decreased quickly, and slow removal from the fine-grained sand resulted in effluent gas concentrations that decreased gradually, resulting in long-term tailing. The long-term tailing was mainly due to diffusion from the fine-grained sand layer to the coarse-grained sand zone. Modeling results are also presented in Figure 11b. As shown, an analytical solution for a one-dimensional advection and a first-order mass transfer model matched the tailing well with two fitting parameters. Given detailed knowledge of the permeability field and initial CT distribution, we were also able to predict the effluent concentration tailing and gas concentration profiles at sampling ports using a numerical

simulator assuming equilibrium CT evaporation. The numerical model predictions were accurate within the uncertainty of independently measured or literature derived parameters. The results demonstrate that proper numerical modeling of CT removal through SVE can be achieved using equilibrium evaporation of NAPL if detailed fine-scale knowledge of the CT distribution and physical heterogeneity is incorporated into the model. However, CT removal could also be fit by a first-order mass transfer analytical model, potentially leading to an erroneous conclusion that the long-term tailing in the experiment was kinetically controlled due to rate-limited NAPL evaporation. Further details of these results were published in Journal of Contaminant Hydrology (Yoon et al., 2009).
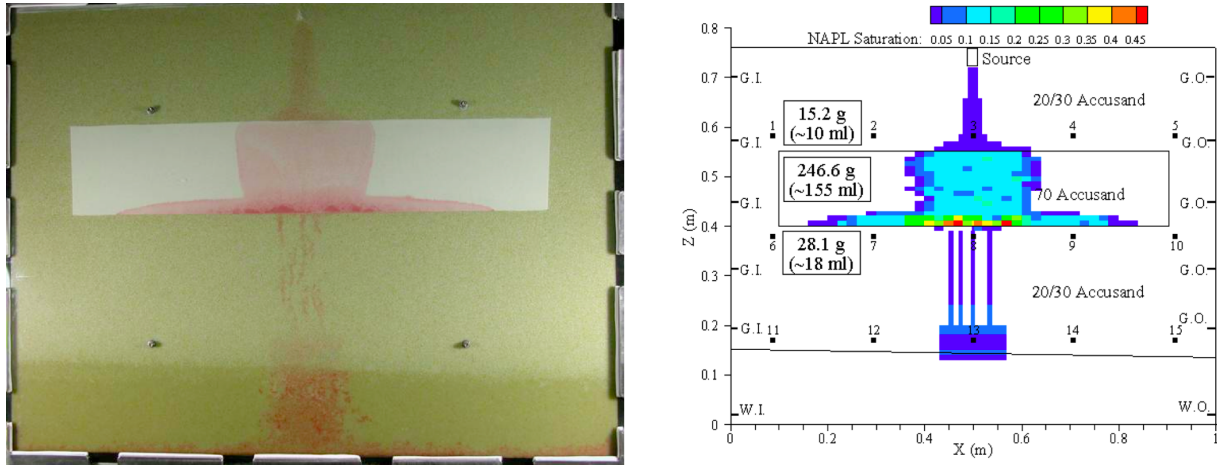

Figure 10. a) Photograph of initial CT distribution in the flow cell. b) Dual energy gamma radiation image of NAPL saturation distribution in the unsaturated zone before soil vapor extraction.
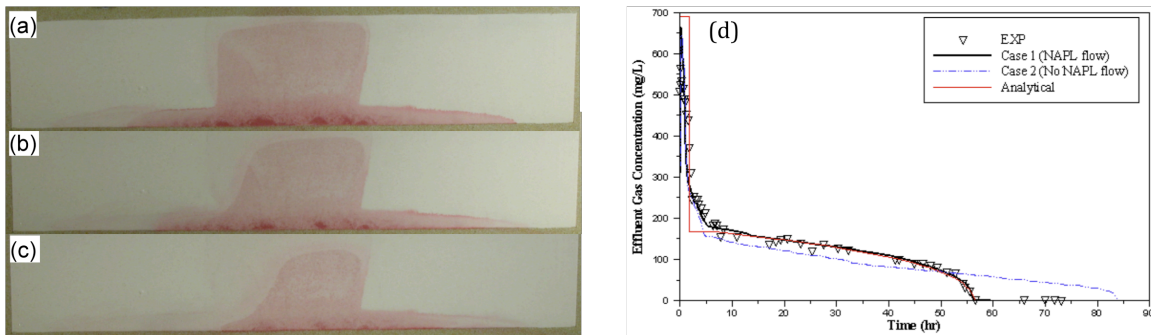

Figure 11. Photographs of DNAPL in the fine sand during SVE after a) 7 hr, b) 20 hr, and c) 34 hr. d) Mesaured and simulated effluent gas concentration profiles. The ratio of longitudinal to transverse dispersion coefficient was 10.

Our laboratory results indicate that the amount, location, and form of NAPL in unsaturated porous media are controlled by the spatial distribution of water saturation and soil permeability, the NAPL spill scenario, water infiltration events, and vapor transport. To evaluate the effects of

these processes at the field scale, we used a new version of STOMP that included a new constitutive model for permeability–liquid saturation–capillary pressure (k–S–P), and we simulated infiltration of NAPL in a 2D domain. We initially considered only pure CT. The new constitutive model considers three NAPL forms: free, residual, and trapped. The 2-D domain contained five stratigraphic layers as shown in Figure 12, and simulations were performed for seven cases. The conceptual model of the soil heterogeneity was based upon the stratigraphy at the Hanford carbon tetrachloride (CT) spill site. Some cases considered co-disposal of NAPL with large volumes of wastewater as also shown in Figure 12; this occurred at the Hanford CT site. In these cases, the form and location of NAPL were most strongly influenced by high water discharge rates and NAPL evaporation to the atmosphere.

Typical results illustrating the location and amounts of each NAPL type are shown in Figure 13. Trapped NAPL only represents a small percentage of the CT at any given time; the remainder is free and residual NAPL. No significant trapped NAPL is present after 38 years, indicating this NAPL type does not affect long-term cleanup. In order to investigate the impact of heterogeneity, the hydraulic conductivity within the lower permeability layer was modeled as a realization of a random field having three different classes. For six extreme cases of 100 realizations, the CT mass that reached the water table varied by a factor of two, and was primarily controlled by the degree of lateral connectivity of the low conductivity class within the lowest permeability layer. The grid size at the top boundary had a dramatic impact on NAPL diffusive flux just after the spill event when the NAPL was present near the ground surface. NAPL evaporation with a fine grid spacing at the top boundary decreased CT mass that reached the water table by 74%, compared to the case with a coarse grid spacing, while barometric pumping had a marginal effect for the case of a continuous NAPL spill scenario considered in this work. For low water infiltration rate scenarios, the distribution of water content prior to a NAPL spill event decreased CT mass that reached the water table by 98% and had a significant impact on the formation of trapped NAPL. For all cases simulated, use of the new constitutive model that allows the formation of residual NAPL increased the amount of NAPL retained in the vadose zone. Density-driven advective gas flow from the ground surface illustrated in Figure 14, controlled vapor migration in strongly anisotropic layers, causing NAPL mass flux to the lower layer to be reduced. These simulations indicate that consideration of the formation of residual and trapped NAPLs and dynamic boundary conditions (e.g., areas, rates, and periods of different NAPL and water discharge and fluctuations of atmospheric pressure) in the context of full three-phase flow are needed, especially for NAPL spill events at the ground surface. In addition, NAPL evaporation, density driven gas advection, and NAPL vertical movement enhanced by water flow must be considered in order to predict NAPL distribution and migration in the vadose zone. Further details of these results are in Journal of Contaminant Hydrology (Yoon et al. 2007).
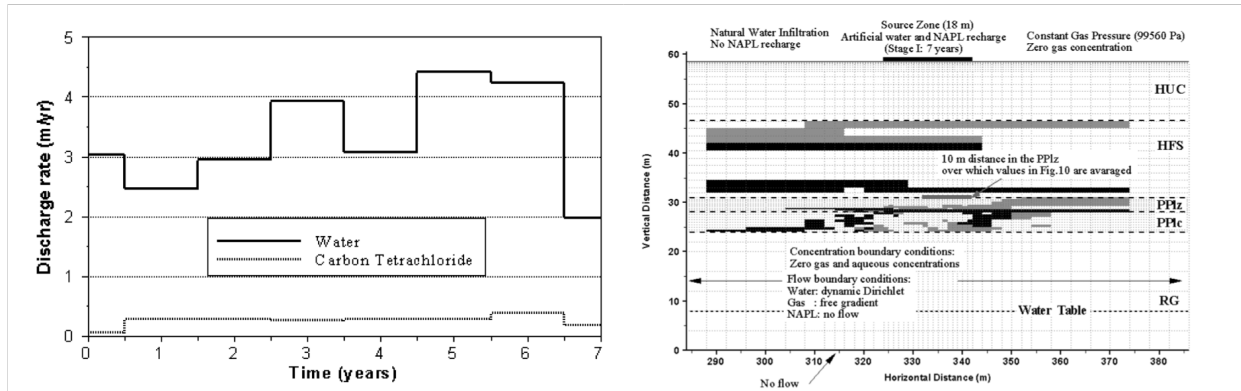
Figure 12. a) Water and NAPL discharge rates for the 216-Z-9 trench at the Hanford site. B) Numerical domain, boundary conditions, and distribution of heterogeneous permeability in stratigraphic units (Case 1). White stands for mean permeability and black and gray colors stand for permeability an order of magnitude lower and higher than a mean value in each layer, respectively. The model domain is 662 m wide by 58.5 deep.
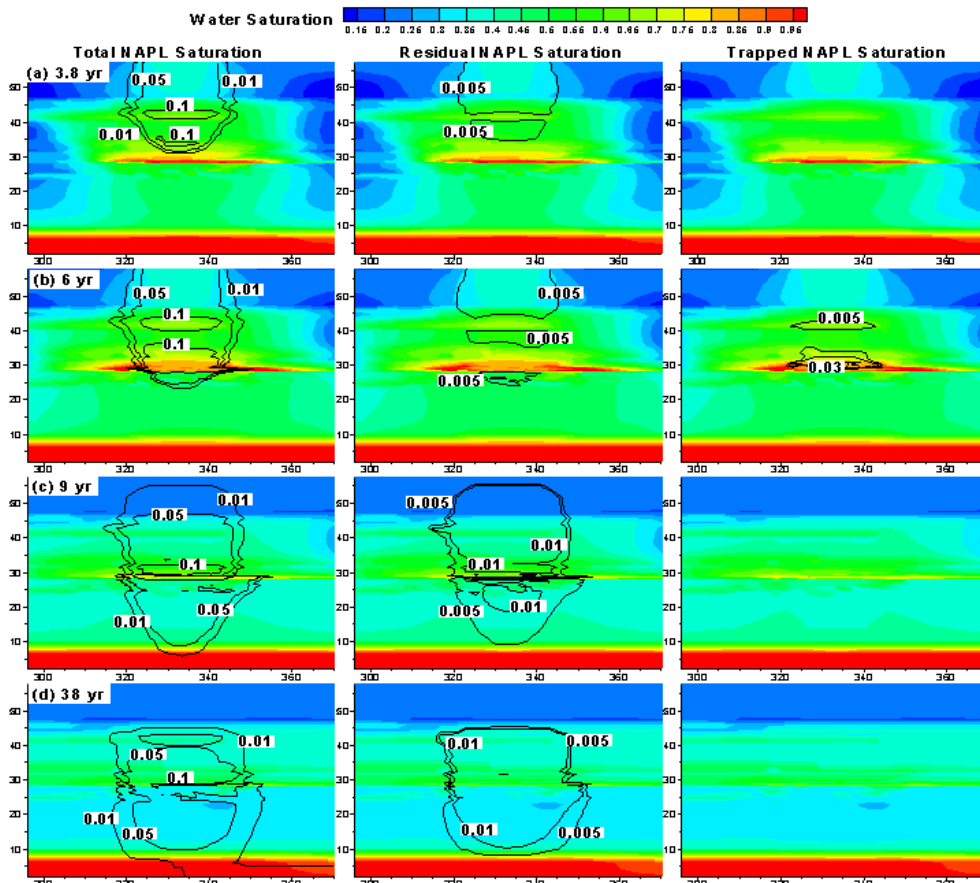

Figure 13. Snapshots of water saturation (color bar), total NAPL saturation, trapped NAPL saturation, and residual NAPL saturation (Case 1) at (a) 3.8 yr, (b) 6 yr, (c) 9 yr, and (d) 38 yr. Contour lines stand for NAPL saturation.
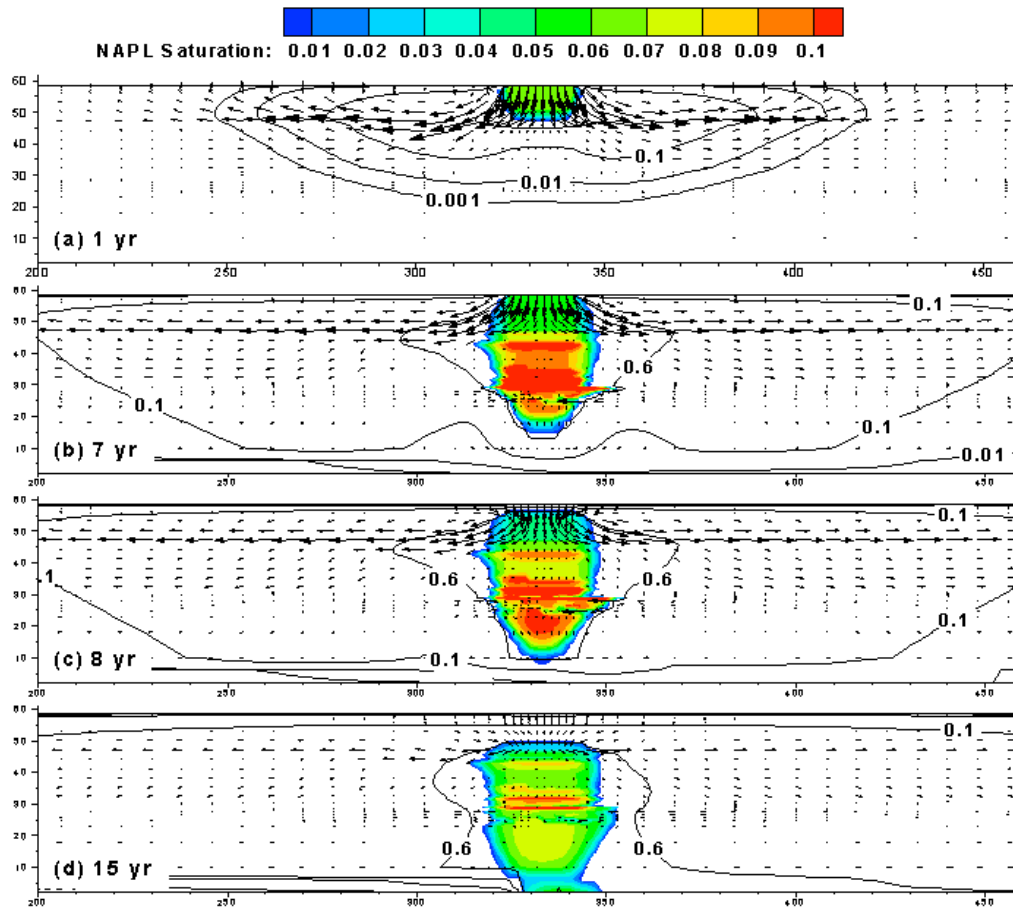
Figure 14. Snapshots of total NAPL saturation (color bar), gas concentration (g/L, contour lines), and gas velocity (vectors) at (a) 1 yr, (b) 2 yr, (c) 7 yr, and (d) 15 yr. Saturated gas concentration is 0.65 g/L. The model domain is 662 m wide. Arrow sizes represent the relative magnitude of the Darcy gas velocities.

The effect of surface-active compounds on NAPL migration and entrapment was also explored using the calibration parameters obtained from model simulations of the CT mixture flow cell experiment. As before, NAPL and wastewater discharge rates and a heterogeneous permeability field representative of the Hanford site were used. Simulation results for the CT mixture are compared to those for pure CT in Figures 15 and 16. In Figure 15, the CT mixture experiences more lateral spreading and residual entrapment than pure CT during infiltration. In Figure 16, we show that this results in 1.5X more of the CT mixture being trapped in the low permeability Plio-Pleistocene unit than the pure CT, and 8 times less of the CT mixture reaching the groundwater table than the pure CT after 38 years of simulation. This is a very large difference and indicates consideration of co-disposed compounds with surface-active properties is critical to accurate prediction of CT migration and entrapment, and the risk that CT poses to groundwater. These results are also being presented in the manuscript by Fitzgerald et al. (2011) that will soon be submitted to Journal of Contaminant Hydrology.
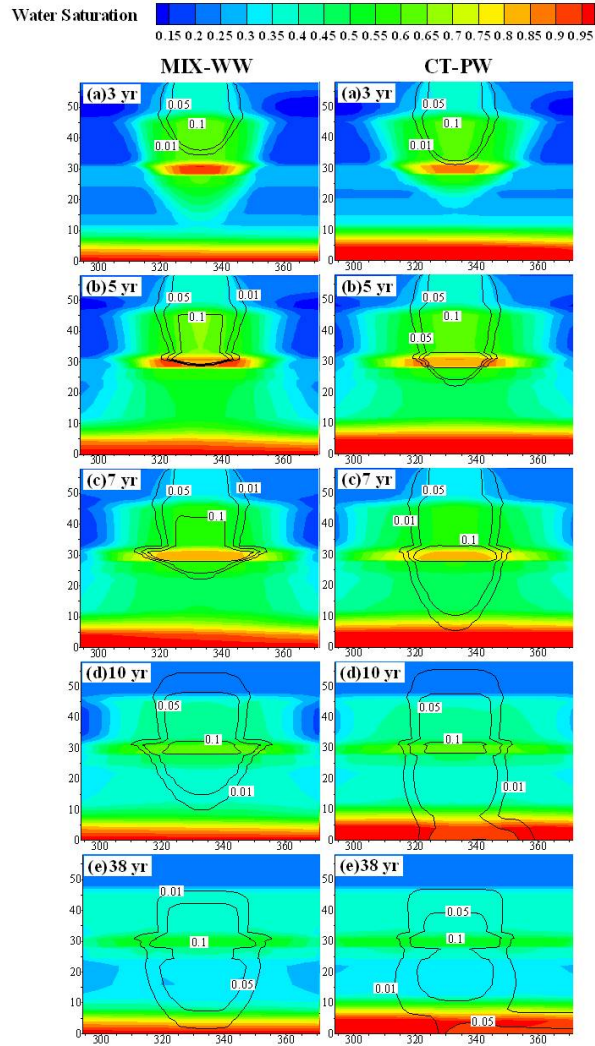
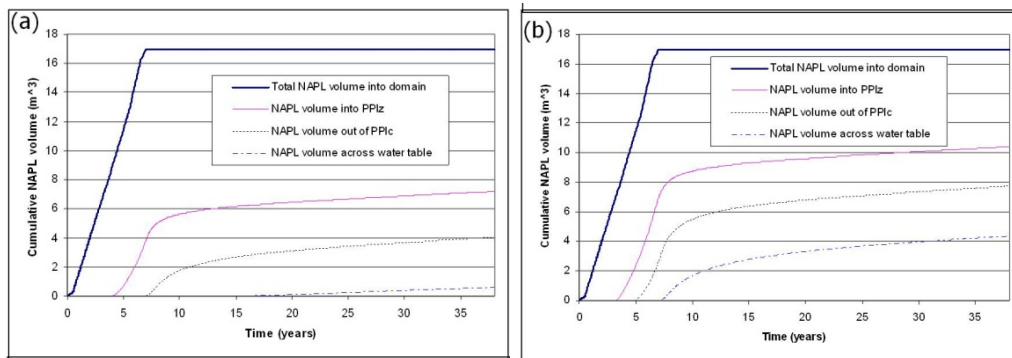Figure 15. Simulated water saturations and NAPL concentrations over time at the model field site.

Figure 16. NAPL volumes across different regions of model domain for the a)mixture and b) pure NAPL.

REFERENCES
(NOTE: * INDICATES PEER-REVIEWED PUBLICATIONS THAT ACKNOWLEDGED DOE FUNDING FROM THIS PROJECT)

Clifford, JS, MA Ioannidis, and RL Legge, Enhanced aqueous solubilization of tetrachloroethylene by a rhamnolipid biosurfactant. J. Colloid and Interface Science, 305: 361-365, 2007.

*Fitzgerald, L., H. Yoon, A.J. Valocchi, C.J. Werth, M. Oostrom, T.W. Wietsma, Impact of NAPL and wastewater properties on DNAPL migration and redistribution in unsaturated porous media, J. Contaminant Hydrology, To be submitted in July, 2011.

Last, GV, VJ Rohay, Refined Conceptual Model for the Volatile Organic Compounds-Arid Integrated Demonstration and 200 West Area Carbon Tetrachloride Expediated Response Action. PNL-8597/UC-630, DOE/RL-91-58, Pacific Northwest Laboratory, 1993.

*Nellis, SR. Effect of mixture properties and aging on soil wettability at the Department of Energy's Hanford site. M.S. Thesis. University of Illinois at Urbana-Champaign, Urbana, IL, 2008.

*Nellis, S.R., Yoon, H., Werth, C.J., Oostrom, M., and Valocchi, A.J., Surface and interfacial properties of Nonaqueous-Phase Liquid mixtures released to the subsurface at the Hanford Site. Vadose Zone Journal. 8(2): 343-351, 2009.

Ng, K.M., A.C. Payatakes, Stochastic simulation of the motion, breakup, and stranding of oil ganglia in water-wet granular porous media during immiscible displacement, 26(3), 419-429 1980.

Oostrom, M, F Zhang, VL Freedman, GD Tartakovsky. Improved Predictions of Carbon Tetrachloride Contaminant Flow and Transport: Implementation of Kinetic Volatilization and Multicomponent NAPL Behavior. PNNL-17878, Pacific Northwest National Lab., 2008.

Rohay, VJ, KJ Swett, GV Last, Conceptual Model of the Carbon Tetrachloride Contamination in the 200 West Area at the Hanford Site, WHC-SD-EN-TI-248, Rev. 0, Westinghouse Hanford Company, Richland, Washington, 1994.

*Yoon, H., Valocchi, A.J., and Werth, C.J. 2007. Effect of soil moisture dynamics on dense nonaqueous phase liquid (DNAPL) spill zone architecture in heterogeneous porous media. J. Contaminant Hydrology, 90, 159–183.

*Yoon, H., Oostrom, M., Werth, C.J., Estimation of interfacial tension between multi-component organic mixtures and water. Environmental Science & Technology. 43(20): 7754–7761, 2009.

*Yoon, H., Oostrom, M., Wietsma, T., Werth, C.J., Valocchi, A.J., Numerical and experimental investigation of DNAPL removal mechanisms in a layered porous medium by means of soil vapor extraction. J. Contaminant Hydrology. 109: 1-13, 2009.

*Yoon, H., A.J. Valocchi, C.J. Werth, T. Dewers, Pore-scale simulation of mixing-induced calcium carbonate precipitation and dissolution in a microfluidic pore network, Water Resources Research, To be submitted in July, 2011.

*Zhang, C., K. Dehoff, N. Hess, M. Oostrom, T.W. Wietsma, A.J. Valocchi, B.W. Fouke, C.J. Werth, A pore scale study of transverse mixing induced CaCO3 precipitation and permeability reduction in a model subsurface sedimentary system, Environmental Science and Technology, 44(20), 7833-7838, 2010.

THESES THAT ACKNOWLEDGED DOE FUNDING FROM THIS PROJECT

Scott Nellis, M.S. thesis, UIUC, 2008, Effect Of Mixture Properties And Aging On Soil Wettability At The Department Of Energy's Hanford Site.

Garvin Prescod, M.S. thesis, UIUC, 2008, Methods for Fabrication of Microfluidic Systems to Evaluate Multi-Phase Fluid Behavior in Porous Media.

Karl Dehoff, M.S. Thesis, UIUC, 2010, Pore-Scale Characterization Of Transverse Mixing-Induced Calcium Carbonate Precipitation Of Relevance To Geological Carbon Sequestration.

CONFERENCE PRESENTATIONS THAT ACKNOWLEDGED DOE FUNDING FROM THIS PROJECT

Yoon, H., Valocchi, A.J., and Werth, C.J. (ABSTRACT) Effects of Soil Moisture Dynamics on NAPL Spill Zone Architecture in Two-Dimensional and Three-Dimensional Heterogeneous Porous Media, Eos Trans. AGU, 88(23), Jt. Assem. Suppl., Abstract H31A-05, 2007.

Yoon, H., Valocchi, A.J., Werth, C.J., and Oostrom, M (ABSTRACT) Numerical investigation of NAPL Source Zone Architecture in Two-Dimensional and Three- Dimensional Unsaturated Porous Media, Eos Trans. AGU, 88(52), Fall Meet. Suppl., Abstract H33H-1732, 2007.

Yoon, H., Werth, C.J., Valocchi, A.J., and Oostrom, M. Impact of multiphase flow and transport on NAPL distribution and NAPL removal mechanisms in unsaturated porous media, Fall Meeting, Abstract H41C-0895, 2008.

Werth, C.J., Valocchi, A.J., Oostrom, M., Yoon, H., and Zhang, C. (ABSTRACT) Physical and Chemical Properties that Give Rise to Flow ByPassing in DNAPL Impacted Groundwater Source Zones, Fall Meeting, Abstract H33J-08, 2008.

Dehoff, K., Zhang, C. Y., Werth, C. J. Pore-Scale Study of Mixing Induced Precipitation and Permeability Reduction. American Geophysical Union Fall Meeting: San Francisco, CA, 15 - 19 December 2008.

Dehoff, K., Yoon, H., Zhang, C., Valocchi, A. J., Werth, C. J. Numerical and Experimental Investigation of Mixing-Induced Calcite Precipitation and Permeability Changes in Micromodel Experiments. American Geophysical Union Fall National Meeting, San Francisco, CA, 2009.

Yoon, H., Oostrom, M, Wietsma, T. W., Valocchi, A. J., Werth, C. J. Numerical and Experimental Investigation Of The Impact of Organic Chemical Mixtures on DNAPL Migration and Distribution in Unsaturated Porous Media. American Geophysical Union National Fall Meeting, San Francisco, CA. 2009.

Zhang, C., K. DeHoff, A. Valocchi, M. Oostrom, T. Wietsma, C.J. Werth, Pore-scale investigation of the impacts of solution chemistry on mixing-induced mineral precipitation, American Chemical Society National Spring Meeting, San Francisco, CA, 2010.